OPEN ACCESS
IOP Publishing
Plasma Physics and Controlled Fusion
Plasma Phys. Control. Fusion **64** (2022) 045012 (6pp)
https://doi.org/10.1088/1361-6587/ac4853

Scissor-cross ionization injection in laser wakefield accelerators

Jia Wang[1,2], **Ming Zeng**[1,2,*], **Xiaoning Wang**[1,2], **Dazhang Li**[1,2,*] **and Jie Gao**[1,2]

[1] Institute of High Energy Physics, Chinese Academy of Sciences, Beijing 100049, People's Republic of China
[2] University of Chinese Academy of Sciences, Beijing 100049, People's Republic of China

E-mail: zengming@ihep.ac.cn and lidz@ihep.ac.cn

Received 8 October 2021, revised 27 November 2021
Accepted for publication 5 January 2022
Published 18 February 2022

Abstract

We propose to use a frequency-doubled pulse colliding with the driving pulse at an acute angle to trigger ionization injection in a laser wakefield accelerator. This scheme effectively reduces the duration of the injection; thus, high injection quality is obtained. Three-dimensional particle-in-cell simulations show that electron beams with energy of ∼500 MeV, a charge of ∼40 pC, energy spread of ∼1% and normalized emittance of a few millimeter milliradian can be produced by ∼100 TW laser pulses. By adjusting the angle between the two pulses, the intensity of the trigger pulse and the gas doping ratio, the charge and energy spread of the electron beam can be controlled.

Keywords: laser acceleration, plasma accelerator, electron injection

(Some figures may appear in colour only in the online journal)

The laser wakefield accelerator (LWFA) proposed by Tajima and Dawson has attracted considerable attention due to its orders-of-magnitude higher acceleration gradient than those of the conventional radio-frequency accelerators [1]. Great breakthroughs have been made in the past few years. For example, an electron beam with energy of 7.8 GeV has been generated at 20 cm [2]. Electron beams with energy spread at the sub-percentage level have been produced using density-tailored plasma [3]. The 24 h stable LWFA has been achieved by decoding sources of energy drift and jitter [4]. Improving the output beam quality parameters, including the energy spread, the beam charge, the emittance, the energy stability and so on, has been a long-term goal in this society for high-demanding applications, such as plasma-based light sources and colliders [5–8].

To optimize the output beam quality, many controlled injection schemes have been proposed, such as pulse collision injections [9–11], density gradient injections [12–14], ponderomotive injections [15, 16], external magnetic field injections [17–20] andionization injections [21–24]. Ionization injection releases electrons inside the pseudo-potential well of a wakefield by high-order ionization of the dopant species (high-Z elements, such as nitrogen, oxygen, neon or argon). The injection amount can be adjusted by changing the density ratio of the dopant to the background plasma, which is pre-ionized from low-ionization-threshold species, such as hydrogen and helium. Ionization injection has the advantage of high reproducibility, but its energy spread is usually large. To reduce the energy spread, one may use the self-dechirping effect [3, 25] and/or reduce the electron's injection length [26, 27]. For example, an electron beam with slice energy spread of 13 keV and a charge of 0.4 pC can be produced by ionization injection of a counter-propagating laser pulse [28]. An electron beam with slice energy spread of 12 keV and a charge of 5 pC can be produced by two colliding lasers propagating in the transverse direction [29]. A scheme of beat frequency ionization injection using a frequency tripled laser was proposed to generate low-energy-spread electron

* Authors to whom any correspondence should be addressed.

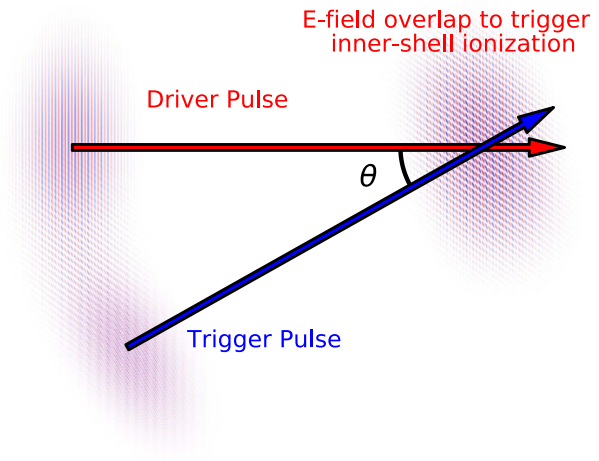

Figure 1. An illustration of scissor-cross ionization injection. When the driver pulse and trigger pulse overlap in the plasma, a strong transient electric field is generated, which ionizes the inner shell electrons of the dopant atoms and produces ionization injection.

beams [30, 31]. However, this scheme has experimental difficulties due to the lack of a high-efficiency frequency tripler.

In this work, we propose a new scheme to trigger electron ionization injection by a frequency-doubled pulse colliding with the driver pulse at an acute angle, as illustrated in figure 1. A driver laser pulse drives a plasma wake (not shown in the figure) and collides with a trigger laser pulse at an angle θ. During the collision, a higher superimposed electric field is generated, triggering the ionization of electrons of the inner shell of the dopant species. The driving laser itself cannot ionize the inner shell of the dopant. The ionization injection only occurs when two laser pulses overlap, thus the injection is localized and the energy spread of the produced electron beam is limited. The frequency-doubled trigger laser has largely reduced ponderomotive force compared to a fundamental-frequency trigger laser with the same ionization electric field strength; thus, its disturbance to the main wakefield is limited. The trajectories of the driver and trigger lasers are similar to the two blades of a pair of scissors; thus, we call this scheme the scissor-cross ionization injection.

Snapshots of the example two-dimensional (2D) particle-in-cell (PIC) simulation using the code WarpX [32] are shown in figure 2. In the plots, n_0 is the unperturbed plasma density, ρ_e is the density of background electrons, ρ_d is the density of electrons ionized from the dopant species, E_L is the electric field of the laser pulsesand e is the elementary charge. In the simulation, the background plasma is fully pre-ionized gas (e.g. hydrogen or helium) and the dopant is neon pre-ionized to $+8$ charge state. Because the ionization threshold of Ne^{8+} is $\sim$16.5 TV m^{-1}, for the driver pulse with normalized vector potential amplitude $a_0 < 4$, it can be guaranteed that Ne^{8+} will not be further ionized by the driver pulse, where $a_0 \approx 8.5 \times 10^{-10}\lambda\,[\mu\mathrm{m}]\sqrt{I_0\,[\mathrm{W\,cm^{-2}}]} = E_0\left[\mathrm{TV\,m^{-1}}\right]\cdot\lambda\,[\mu\mathrm{m}]\,/3.2$ is the normalized vector potential amplitude, I_0 is the laser intensity and E_0 is the peak electric field strength of the laser. Meanwhile, by choosing $a_0 \gtrsim 3$, we ensure the self-guiding of the driver laser pulse for a sufficiently longer electron acceleration distance without using a parabolic plasma channel [33, 34]. Practically, the plasma has a linear up-ramp from $z = -30$ μm to 0, followed by a plasma density plateau with $n_0 = 1.63 \times 10^{18}$ cm^{-3}. The driver pulse has a normalized vector potential amplitude of $a_0 = 3.24$ and a wavelength of 800 nm, while the trigger pulse has a normalized vector potential amplitude of $a_1 = 1.62$ and a wavelength of 400 nm. Both pulses have a spot radius of $r_0 = r_1 = 15$ μm and pulse duration of 30 fs. Their focusing is synchronized spatially and temporally to trigger the inner-shell ionization of the dopant species, which starts at the instant of time shown in figure 2(a). The superimposed peak electric field, and thus the inner shell ionization probability, reach their maxima at the instant of time shown in figure 2(b), leading to considerable trapping of the ionized electrons and formation of an electron beam, as shown in figure 2(c). After the collision finishes, ionization injection no longer occurs, because the electric field strength does not reach the inner-shell ionization threshold of the dopant species, even if the self-focusing of the driver laser pulse occurs, as shown in figure 2(d): i.e. ionization injection only occurs when two laser beams overlap, which ensures a limited injection distance. For comparison, we also performed another simulation with the trigger pulse turned off, which has no injection because the electric field is always below the inner-shell ionization threshold, shown as the black solid line in figure 2(d).

To study the effects of different collision angles, we performed simulations with θ varying from 10° to 150°. The snapshots and the quality of the injected beams are shown in figures 3 and 4, respectively. These simulations use a pure neon element, which provides both the pre-ionized outer shell to form the background plasma and the bounded inner shell for ionization injection. As one can see, the beam quality changes with θ. For $\theta \lesssim 30°$, the disturbance of the trigger pulse to the main wakefield is small, but the length of the region that the two pulses overlap, and thus the injection length, which can be estimated by $r_0/\tan\theta$, is relatively large. For $\theta \gtrsim 60°$, the injection length can be $\sim$10 μm, but there is a significant disturbance of the trigger pulse to the main wakefield, which degrades the injected beam quality. Moreover, for $\theta \lesssim 30°$, the injection mechanism is purely ionization injection while, for $\theta \gtrsim 60°$, the injection mechanism is gradually switched to colliding pulse injection, as shown in figure 4(a). The phase space distribution of the output beam for $\theta = 30°$ is plotted in figure 4(b), which shows a beam with a mean energy of 578 MeV, a root-mean-square (RMS) energy spread of 0.7% and a normalized emittance of 4.7 mm·mrad. The emission angle and energy correlation in figure 4(a) is caused by the asymmetric initialization of the electrons and the ponderomotive force of the oblique incident trigger pulse disturbing the wakefield bubble and the electrons.

Obviously, the strength of the superimposed electric field of the driver and trigger does not depend on their sizes. However, the sizes of the pulses determine the injection quantity and also the injection difficulty in a real experiment. We discuss the effect of changing the trigger size in the following. Assumeing that the wakefield is a spherical bubble, the pseudo-potential

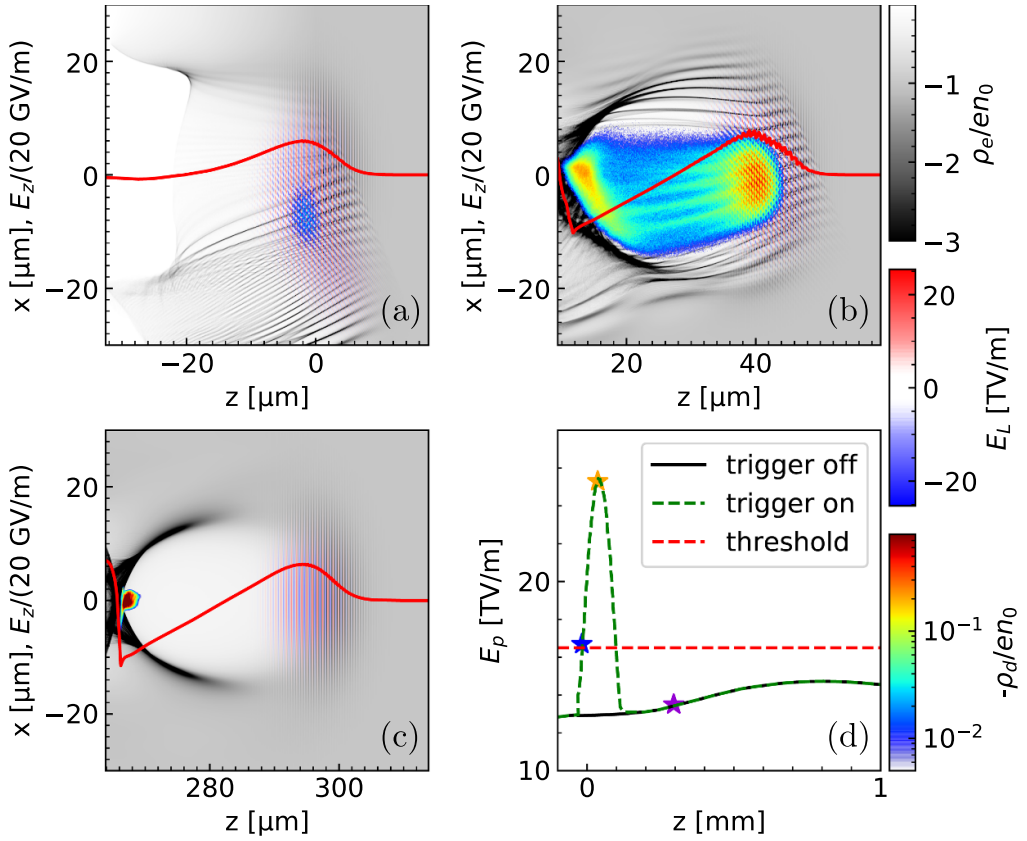

Figure 2. Snapshots of a 2D PIC simulation using the scissor-cross ionization injection scheme: (a) at the instant of time that the driver and trigger pulses overlap and the inner-shell ionization of the dopant starts, (b) when the superimposed peak electric field reaches its maximum, and (c) at a certain acceleration distance. The red curves show the line-out of the axial longitudinal electric field E_z in units of 20 GV m^{-1}. (d) The peak electric field (E_p) vs. the position of the driver pulse with the trigger pulse turned on (green dashed line) and off (black solid line). The red dashed line represents the ionization threshold of Ne^{8+}. The blue, orange and violet stars correspond to the positions that snapshots (a)–(c) are taken, respectively.

in the bubble can be estimated by $\psi \approx \omega_p^2(r_b^2(\zeta) - r^2)/4c^2$, where r_b is the bubble radius, r is the distance to the central axis, $\zeta = z - ct$ is the co-moving coordinate, c is the speed of light in vacuum, $\omega_p = c\sqrt{4\pi r_e n_0}$ is the plasma frequency and r_e is the classical electron radius [35, 36]. The trapping conditions for an electron are $\Delta\psi \lessapprox -1$ if the electron has negligible initial momentum [16]. In a plasma with the density $n_0 = 1.63 \times 10^{18}$ cm^{-3}, the laser with $a_0 = 3.24$ and the matched spot size $r_0 = 3.6c/\omega_p = 15$ μm drives a wakefield with its distribution of pseudo-potentials, as illustrated in figure 5(a). The electrons being ionized in the dashed red circle satisfy the trapping conditions and can be captured by the wakefield. A larger spot size and longer pulse duration of the trigger can decrease the influence of the time delay jitter of the two pulses to the output electron beam energy, as seen in figure 5(b). This is because the time delay jitter of a smaller trigger laser more significantly influences the injection phase of the electron beam, which determines the acceleration field strength exerted on the beam.

We also performed fully three-dimensional (3D) simulations to verify our scheme. Because the laser spot size evolutions in 2D slab and 3D geometries are different, even with the same laser parameters [26, 37], we use modified parameters in the 3D simulation as follows to avoid the overshoot of self-focusing, which introduces undesired ionization injection and degrades the injection quality. The driver and trigger pulses have normalized vector potential amplitudes of $a_0 = 2.74$ and $a_1 = 1.37$, respectively, and they have the same focal waist radius of $r_0 = r_1 = 20$ μm. They are both polarized in the y direction and collide at $\theta = 8°$. We do not choose $\theta = 30°$ as in figure 4(b) because a larger θ significantly increases the computational cost to an unaffordable level. The pre-ionized background plasma density is $n_0 = 1.36 \times 10^{18}$ cm^{-3} and the density of Ne^{8+} is $n_0/8$. The simulation shows that the maximum electric field strength after the occurrence of self-focusing is 15 TV m^{-1}, which is sufficiently smaller than the ionization threshold of Ne^{8+} (which is around 16.5 TV m^{-1}); thus, the driver pulse itself does not trigger ionization injection. The simulation has a moving window size of (100 μm, 100 μm, 50 μm) and a cell number of (768, 128, 2432) for the (x, y, z) directions, respectively. The results are shown in figure 6. The electron beam is injected by our scheme at $t = 1.0$ ps with a small absolute energy spread (figure 6(a)) and mainly experiences positive chirping during the acceleration (figure 6(b)).

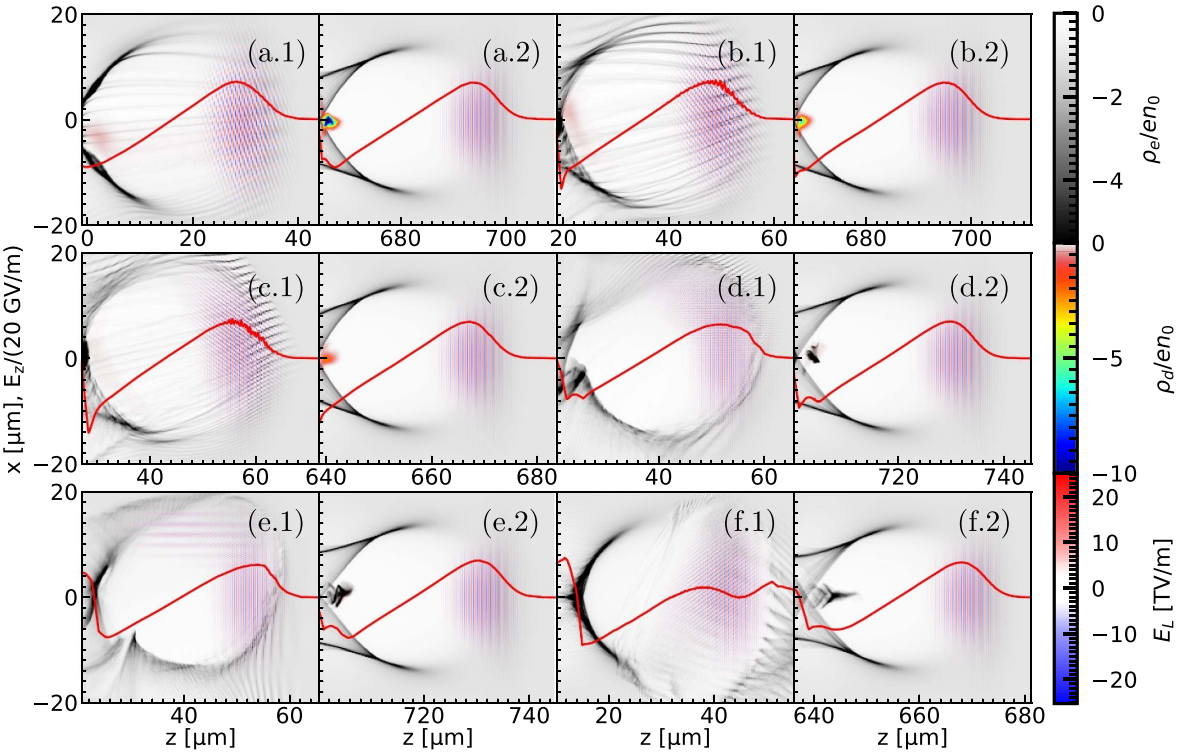

Figure 3. Snapshots of simulations with the collision angles (a.1, 2) $\theta = 10°$, (b.1, 2) $\theta = 20°$, (c.1, 2) $\theta = 30°$, (d.1, 2) $\theta = 60°$, (e.1, 2) $\theta = 90°$ and (f.1, 2) $\theta = 150°$. The snapshots when the two pulses collide are (x.1) and the snapshots after certain acceleration distances are (x.2), where x stands for the letters from (a) to (f). The line-out of the axial longitudinal electric field E_z is plotted as red curves in the subplots.

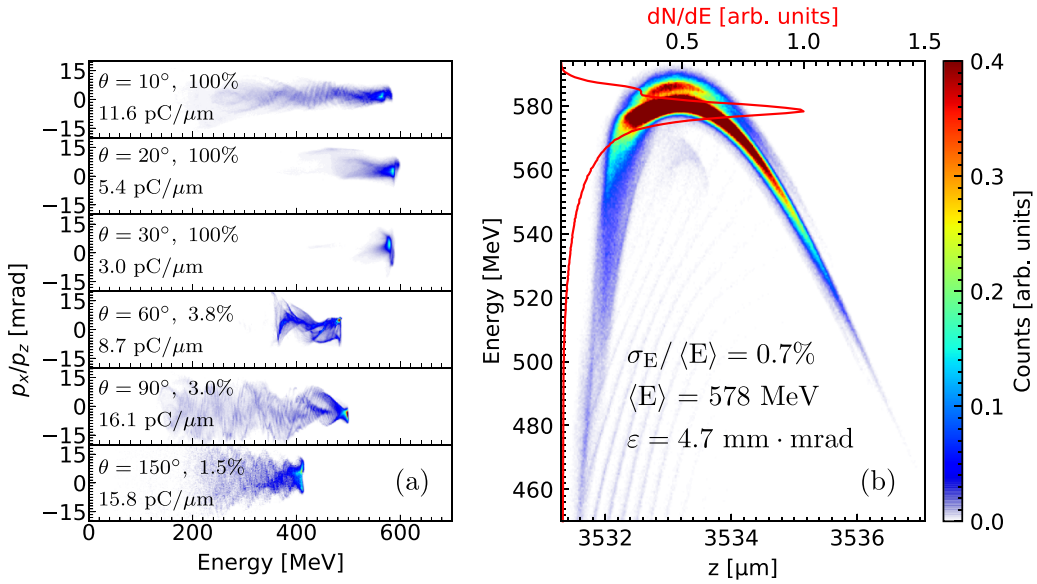

Figure 4. (a) The energy and angular distribution of electron bunches with different collision angles θ. The percentages in the legend show the ratios of the charge from the inner-shell of the dopant species (i.e. from ionization injection) to the total injected charge, and the charges in units of pC μm^{-1} (because of the 2D slab geometry) are also shown. The ratio of transverse momentum to longitudinal momentum p_x/p_z represents the divergence angle of the beam. (b) The phase space distribution of the electron beam at the acceleration distance of 3.5 mm for $\theta = 30°$. The beam quality parameters are shown in the plot: the mean energy is $\langle E \rangle = 578$ MeV, the RMS energy spread is $\sigma_E/\langle E \rangle = 0.7\%$ and the transverse normalized emittance is $\varepsilon = 4.7$ mm·mrad.

At the acceleration distance of about 4 mm (figure 6(c)), the electron beam enters the negative chirping region due to the weakening of the driver; thus, the initial small absolute energy spread is retrieved (the phase space is shown in figure 6(d)). The beam after the acceleration distance of 4 mm has a charge of $Q = 40$ pC, a peak current of $I_{peak} = 6.22$ kA, a mean energy

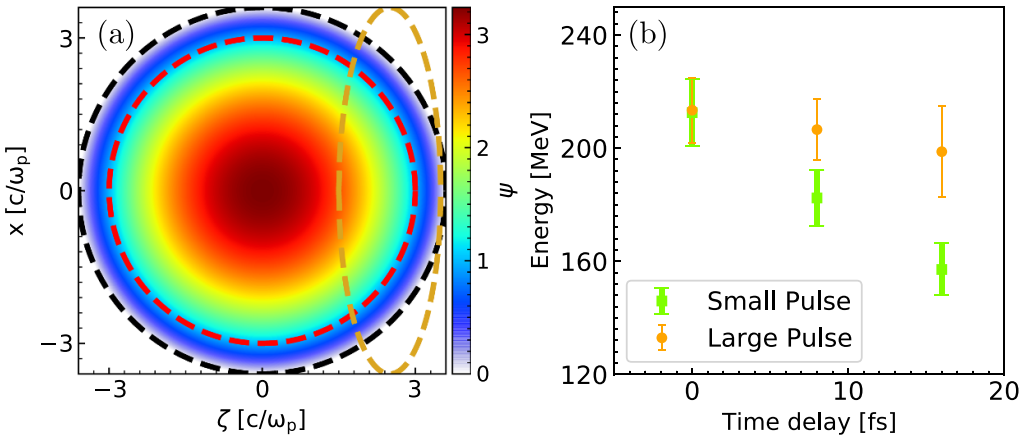

Figure 5. (a) An illustration of pseudo-potential distribution in the co-moving frame of the driver laser. The driver laser has $a_0 = 3.24$ and $r_0 = 15$ μm, and the plasma density is 1.63×10^{18} cm^{-3}. The black dashed curve represents the boundary of the bubble and the dashed red curve encircles the region of inner-shell ionization in which it is possible to satisfy the trapping condition $\Delta\psi \leqslant -1$. The golden ellipse represents the profile of the driver laser, which is propagating towards the $+\zeta$ direction. (b) The mean energy (dots) and energy spread (vertical error-bars) vs. time delay of the trigger pulse relative to the driver for two cases of the trigger sizes obtained by 2D PIC simulations. Here, a_1 is fixed to 1.62 for the trigger laser, the dopant Ne^{8+} density is fixed to 3% of the pre-ionized plasma density, the acceleration distance is fixed to 1 mm and the collision angle is fixed to $\theta = 8°$. The orange symbols represent the case with a larger trigger spot size $r_1 = 15$ μm and a longer trigger pulse duration $\tau_1 = 30$ fs, and the green symbols represent the case with a smaller trigger spot size $r_1 = 3$ μm and a shorter trigger pulse duration $\tau_1 = 6$ fs.

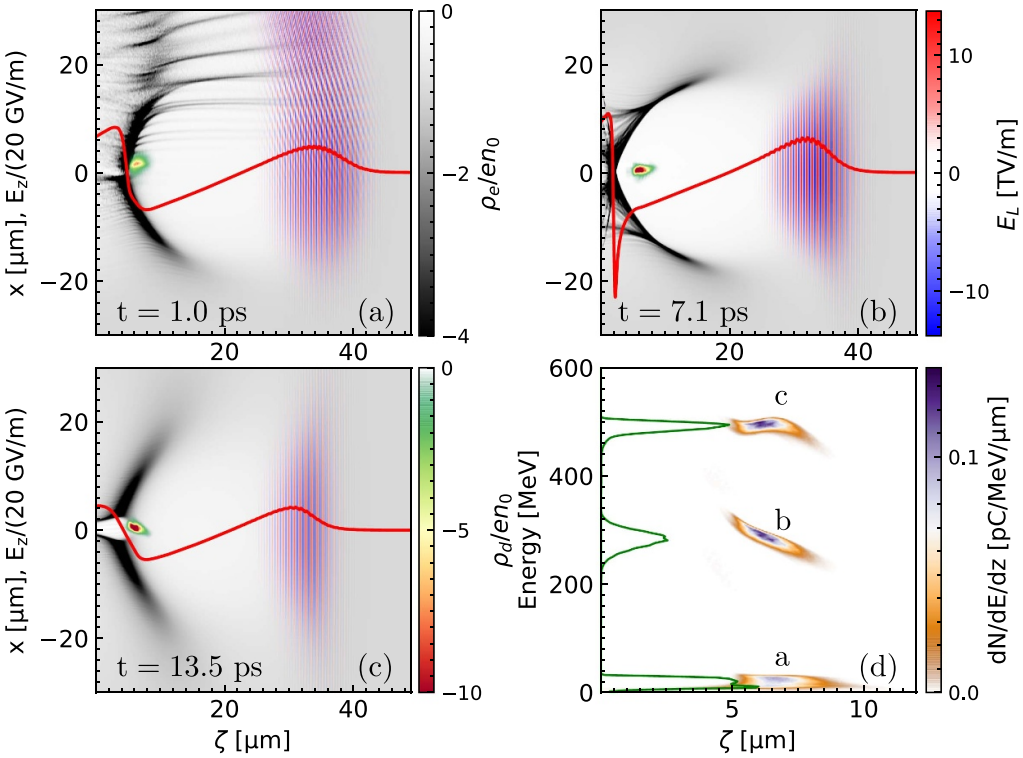

Figure 6. Plots of a 3D PIC simulation. The driver pulse has $a_0 = 2.74$, the trigger pulse has $a_1 = 1.37$, and the collision angle is $\theta = 8°$. The snapshots are taken (a) shortly after colliding, (b) at about 2 mm acceleration distance and (c) at about 4 mm acceleration distance. (d) The phase space distribution and energy spectrum (green curves) of the trapped electron beam at the time corresponding to the above three snapshots.

of $\langle E \rangle = 500$ MeV, an RMS energy spread of $\sigma_E / \langle E \rangle = 1.6\%$ and normalized emittance of $\varepsilon_x = 1.11$ mm·mrad, $\varepsilon_y = 7.84$ mm·mrad for the two transverse directions, respectively.

In conclusion, we have introduced a scissor-cross ionization injection scheme in an LWFA, which uses the intense electric field generated at the moment when the trigger pulse overlaps with the driver laser pulse to ionize the inner shell

electrons of the dopant species and to trigger ionization injection. Both 2D and 3D simulations show that this scheme produces high-quality electron beams with an energy spread of the order of 1%. The ionization injection is limited to a small region with a length of $\sim r_0/\tan\theta$, which is typically $\lesssim 100\ \mu$m, where r_0 is the spot size of the driver pulse and θ is the collision angle. It is theoretically possible to further decrease the energy spread to the per-mille level by slightly increasing θ and/or by increasing the acceleration distance with a preformed plasma channel. Although the 2D slab geometry is different from the 3D geometry, it is reasonable to trust the 2D conclusion that a moderate acute collision angle is optimal, which balances the contradiction between a short injection length and a small disturbance to the injected electron beam.

In experimental implementation of this scheme, the trigger pulse can be replaced by a laser with any frequency, as long as the superimposed electric field exceeds the inner-shell ionization threshold of the dopant species when the two pulses collide. However, with a certain peak electric field strength, a lower-frequency laser has larger ponderomotive force, which may degrade the injection quality. We mainly use the frequency-doubled trigger in our discussion, due to its reasonable experimental difficulty and relatively small ponderomotive disturbance to the main wakefield. The timing requirement of this scheme is ∼20 fs, as shown in figure 5(b), which is much more relaxed than that which is achievable in state-of-the-art experiments (∼3 fs) [11, 38].

Data availability statement

The data that support the findings of this study are available upon reasonable request from the authors.

Acknowledgments

This work is supported by the Research Foundation of the Institute of High Energy Physics, Chinese Academy of Sciences (Grant Nos. E05153U1, E15453U2, Y9545160U2 and Y9291305U2). This research used the open-source particle-in-cell code WarpX, primarily funded by the US DOE Exascale Computing Project. We acknowledge all the WarpX contributors.

ORCID iDs

Jia Wang https://orcid.org/0000-0003-2341-5201
Ming Zeng https://orcid.org/0000-0002-1357-640X
Xiaoning Wang https://orcid.org/0000-0002-2123-3167
Dazhang Li https://orcid.org/0000-0001-6412-8853

References

[1] Tajima T and Dawson J M 1979 *Phys. Rev. Lett.* **43** 267
[2] Gonsalves A J *et al* 2019 *Phys. Rev. Lett.* **122** 084801
[3] Ke L T *et al* 2021 *Phys. Rev. Lett.* **126** 214801
[4] Maier A R *et al* 2020 *Phys. Rev.* X **10** 031039
[5] Leemans W and Esarey E 2009 *Phys. Today* **62** 44
[6] Assmann R W *et al* 2020 *Eur. Phys. J. Spec. Top.* **229** 3675–4284
[7] Wang W *et al* 2021 *Nature* **595** 516–20
[8] Zeng M and Seto K 2021 *New J. Phys.* **23** 075008
[9] Fubiani G, Esarey E, Schroeder C B and Leemans W P 2004 *Phys. Rev.* E **70** 016402
[10] Davoine X, Lefebvre E, Rechatin C, Faure J and Malka V 2009 *Phys. Rev. Lett.* **102** 065001
[11] Golovin G *et al* 2018 *Phys. Rev. Lett.* **121** 104801
[12] Brantov A V, Esirkepov T Z, Kando M, Kotaki H, Bychenkov V Y and Bulanov S V 2008 *Phys. Plasmas* **15** 073111
[13] Geddes C G R, Nakamura K, Plateau G R, Toth C, Cormier-Michel E, Esarey E, Schroeder C B, Cary J R and Leemans W P 2008 *Phys. Rev. Lett.* **100** 215004
[14] Schmid K, Buck A, Sears C M S, Mikhailova J M, Tautz R, Herrmann D, Geissler M, Krausz F and Veisz L 2010 *Phys. Rev. ST Accel. Beams* **13** 091301
[15] Umstadter D, Kim J K and Dodd E 1996 *Phys. Rev. Lett.* **76** 2073
[16] Zeng M, de la Ossa A M and Osterhoff J 2020 *New J. Phys.* **22** 123003
[17] Vieira J, Martins S F, Pathak V B, Fonseca R A, Mori W B and Silva L O 2011 *Phys. Rev. Lett.* **106** 225001
[18] Vieira J, Martins J, Pathak V, Fonseca R, Mori W and Silva L 2012 *Plasma Phys. Control. Fusion* **54** 124044
[19] Bulanov S V, Zh T Kando E, M, Koga J K, Hosokai T, Zhidkov A G and Kodama R 2013 *Phys. Plasmas* **20** 083113
[20] Rassou S, Bourdier A and Drouin M 2015 *Phys. Plasmas* **22** 073104
[21] Chen M, Sheng Z-M, Ma Y-Y and Zhang J 2006 *J. Appl. Phys.* **99** 056109
[22] Chen M, Esarey E, Schroeder C B, Geddes C G R and Leemans W P 2012 *Phys. Plasmas* **19** 033101
[23] McGuffey C *et al* 2010 *Phys. Rev. Lett.* **104** 025004
[24] Pak A, Marsh K A, Martins S F, Lu W, Mori W B and Joshi C 2010 *Phys. Rev. Lett.* **104** 025003
[25] Wang W T *et al* 2016 *Phys. Rev. Lett.* **117** 124801
[26] Zeng M, Chen M, Sheng Z-M, Mori W B and Zhang J 2014 *Phys. Plasmas* **21** 030701
[27] Mirzaie M *et al* 2015 *Sci. Rep.* **5** 14659
[28] Wan Y *et al* 2016 *Plasma Phys. Control. Fusion* **58** 034015
[29] Li F *et al* 2013 *Phys. Rev. Lett.* **111** 015003
[30] Zeng M, Chen M, Yu L L, Mori W B, Sheng Z M, Hidding B, Jaroszynski D A and Zhang J 2015 *Phys. Rev. Lett.* **114** 084801
[31] Zeng M, Luo J, Chen M, Mori W B, Sheng Z-M and Hidding B 2016 *Phys. Plasmas* **23** 063113
[32] Vay J-L *et al* 2021 *Phys. Plasmas* **28** 023105
[33] Lu W, Tzoufras M, Joshi C, Tsung F S, Mori W B, Vieira J, Fonseca R A and Silva L O 2007 *Phys. Rev. ST Accel. Beams* **10** 061301
[34] Benedetti C, Schroeder C B, Esarey E and Leemans W P 2012 *Phys. Plasmas* **19** 053101
[35] Kostyukov I, Pukhov A and Kiselev S 2004 *Phys. Plasmas* **11** 5256
[36] Lu W, Huang C, Zhou M, Tzoufras M, Tsung F S, Mori W B and Katsouleas T 2006 *Phys. Plasmas* **13** 056709
[37] Tzeng K-C and Mori W B 1998 *Phys. Rev. Lett.* **81** 104
[38] Yan W *et al* 2017 *Nat. Photon.* **11** 514